POAC'17
Busan, KOREA

Proceedings of the 24th International Conference on
Port and Ocean Engineering under Arctic Conditions
June 11-16, 2017, Busan, Korea

Experimental and Micro-CT study on the Oil Distribution in laboratory grown Sea Ice

Martina Lan Salomon[1], Martin Arntsen[2], Nga Dang Phuong[2], Sönke Maus[1], Megan O' Sadnick[2], Chris Petrich[2], Martin Schneebeli[3], Mareike Wiese[3]

[1] Norwegian University of Science and Technology, Trondheim (NTNU), Norway
[2] Northern Research Institute Narvik (NORUT), Narvik, Norway
[3] WSL Swiss Federal Institute for Snow and Avalanche Research SLF, Davos, Switzerland

ABSTRACT

Increasing activities in Arctic waters bare a risk of oil spills under ice-covered conditions and afford sound understanding of the interplay between sea ice and oil. Towards better knowledge, this study focuses on X-ray- micro computed-tomography (µ-CT) investigations of a laboratory oil- in ice experiment. The 3-dimensional distribution of oil in the porous space of 11- 13 cm columnar ice grown in a laboratory was investigated. Two different oil content measurement methods are discussed. (i) The first method quantifies the oil volume fraction based on µ -CT-scan investigations, allowing spatial oil distribution analysis in the porous space of sea ice. Oil inclusions were mapped manually over the acquired CT-scans with a resolution of 18 µm and 25 µm, respectively. Results give higher oil contents for smaller resolutions. Oil migration of 4 cm was observed. (ii) The second method quantifies the present oil concentration with fluorescent measurements. CT- scans give in comparison to fluorescent measurements a root mean square error of 1.27 % (18 µm) 0.76 % (25 µm), respectively. Bulk salinity determined from melted samples is compared with salinity estimated from µ –CT data.

KEY WORDS: Sea ice, Computer Tomography, Microstructure, Oil, Porosity

INTRODUCTION

Activities in polar marine areas are increasing. Including interest in Arctic resources. Oil exploration in potentially ice-covered regions and growing shipping activities in high latitudes, bare a risk of accidental oil spills. Giving objective to study the interaction of sea ice and oil for environmental and sustainable risk management.

Networks of brine channels and air inclusions make sea ice to a permeable material and a potential entrapment medium for oil. Investigations on the interaction of oil and sea ice have been published since the 1970's (Glaeser & Vance, 1971; NORCOR, 1975). Several field studies and experimental work were conducted since then. Studies were mainly based on destructive two- dimensional observations of thin sections and macroscopic descriptions, characterizing processes from oil encapsulation over oil migration to oil surfacing on sea ice (c.f Martin, 1979; Nelson, 1981; Buist & Pistruzak, 1981; Buist et al., 1983; Otsuka et al. 2004; Karlsson, 2009; Karlsson et al., 2011). Experiments quantifying the oil content in sea ice were conducted by Karlsson et al., (2011) and Otsuka (2004), reporting that the ability of oil to penetrate sea ice is limited by its porosity. A porosity threshold of 0.1 to 0.15 was determined and an oil saturation up to 4.5 to 7 mass percent oil by mass of sea ice was reported. Based on

these observations and model assumptions (Petrich, Karlsson, & Eicken, 2013)) computed the potential oil penetration depth and concluded on oil entrainment volumes from less than 1 L/ m^2 as high as 5 to 10 L/ m^2 with increasing ice temperatures. 3-dimensional insights and application of X-ray tomography (XRT) to sea ice samples were first given by Kawamura (1988) with a resolution of 1 mm. Maus, 2009, 2013, 2015 applied XRT and synchrotron- XRT on sea ice with a resolution of 18 to 25 μm, respectively a resolution of 2 x 5.6 μm. Based on 3- dimensional micro- CT data, oil infiltration rate was computed, concluding on entrainment volume not solely depending on porosity. Furthermore, the control mechanism are described by parameters such as, pore size, pore necking and convection driven desalinization. (Maus et al., 2013) Salomon et al. (2016) give preliminary results on the detection of oil in sea ice based on synchrotron- XRT.

The present experiment was designed to detect the 3-dimensional distribution and the concentration of oil in the porous space of sea ice based on μ -CT investigation. Oil concentration measurements were achieved with two different approaches. (i) First method is based on μ-CT-scans and mapping the oil content over the 2- dimensional μ-CT sections. (ii) Second approach focused on UV-light stimulation and emitted fluorescence measurements of hydrocarbons. Resulted brine volume fraction from μ-CT-scans were converted into bulk salinity and are compared with measured bulk salinity.

METHODS

Experimental Setup

Ice growth was performed in a cold lab at NORUT Narvik in slightly conical double-walled plexiglas container with outer-dimensions of 51 x 51 x 51 cm and inner-dimensions of 50 x 50 x 50 cm. Approximately 100 liter of artificial saltwater (Blue Treasure Synthetic Salt) with an initial salinity of 31.5 ppt was filled into the tank. The plexiglas tank allowed visual access to the freezing process and facilitated the oil injection. The double-tank arrangement, surrounded by a 5 cm thick Styrofoam- isolation and air-cooling allowed one-dimensional ice growth. Heat supply from the bottom of the tank avoided supercooling of the water column and led to columnar ice growth. Fans beneath the tank assured homogenous heat distribution.

Prior to ice growth initiation, artificial seawater had a water temperature of approximately 0 °C. Referred starting point of the experiment is the set of ambient temperature to –15 °C. After 64 hour ice reached a thickness of 8 cm and oil was injected below the ice with a silicon syringe of 5 mm diameter. 28 h hours after oil release, room temperature was raised to -10 °C, to facilitate oil migration, to ensure that the surface temperature well above the nominal pour point of crude oil at -15 °C. Sampling commenced 91.5 hours after experimental start when the ice thickness reached 11-13 cm. Cores were taken with a drill 50 mm in diameter. Samples were stored over night at -80 °C and than transported on dry ice (-78.5 °C) from NORUT Narvik (Norway) to NTNU Trondheim (Norway). After storage at - 50 °C over a period of 9.5 months they were prepared for imaging with X-ray- micro computed-tomography (μ-CT). The cores were cut into subsamples of 2 to 3.5 cm thickness and a diameter of 35 mm. During the cutting process it was attempted to preserve the oil lenses.

During transport from and to WSL Swiss Federal Institute for Snow and Avalanche Research SLF (Davos,Switzerland), where the first μ-CT measurements were performed at -15 °C, sample temperature was kept at the same temperature by eutectic cooling elements. Back to NTNU samples were stored for another 2 months at -50 °C. Imaging of the same samples was conducted at the RECX, Norwegian Centre for X-Ray diffraction, scattering and imaging at

the Norwegian University of Science and Technology (NTNU, Trondheim, Norway). Before imaging was performed samples were warmed up to the imaging temperature of -15 °C over night. Prior to fluorescent measurements sample were molten in airtight glass containers and shipped to NORUT Narvik.

X-ray micro computed- tomography (µ-CT) imaging

µ-CT measurements were conducted with three instruments (i) ScancoMedical AG micro-CT 40 at SLF, (ii) SacancoMedical AG micro-CT 80 at SLF and (iii) XT H 225 ST micro-CT system from Nikon Metrology NV at NTNU. (i & ii) were operated with a micro focus X-ray source (7 µm diameter) current of 177 µA and an acceleration voltage of 45 kV. Detector panels of 2048 x 256 and 2048 x 128 pixels, respectively were used. Tomographic scans were performed in high resolution mode with 2000 rotation per 360°. The height of scans could be chosen according to the sample height. Scans were operated with a field of view (FOV) of 37 mm, resulting in a pixel size of 18 µm. Samples were acquired in a cold- room at ambient temperatures of -15 °C at SLF. Acquisition time at SLF was limited to a window of 5 days, therefore two CTs were used simultaneously. Settings were the same and a difference at the acquisition is not assumed. (iii) a current source of 250 µA and an acceleration voltage of 150 kV. Scans were performed with 3142 rotation per 360°. A Perkin Elmer 1620 with a pixel size of 200 x 200 µm and 2048 x 2018 pixels operated as flat panel detector. The FOV of 50 mm corresponds to a pixel size of 25 µm. Scanning temperature (-15 °C) was controlled with a thermoelectric assembly (www.lairdtech.com) by top and bottom sample cooling.

CT- data provide a 2-d map of the variation of X-ray absorption of substructures within the imaged sea ice. Those 2-d maps are called radiographs and are acquired over a finite number of radiographic viewing directions to reconstruct the distribution of X-ray absorptivity within a horizontal cross-section of the imaged sample. The cross sections are stored as 16-bit grey value stacks and give a 3- dimensional view of the scanned object.The resulting 3-d images of ice cores were processed in ImageJ (rsb.info.nih.gov/ij). First a rectangular cylinder with the largest possible horizontal cross-section was cropped. After cropping a 2 pixel median and 1.5 standard deviation Gaussian blur filter were applied. Segmentation of air and ice was based on using Otsu's algorithm (Otsu, 1979; Maus, 2015) For segmentation of brine from ice the Triangle algorithm was applied (Zack et al., 1977). A different segmentation method was chosen for setting the brine threshold, as the Otsu algorithm was found to give too high brine volumes (Hullar et al., 2016).

Absorption contrast between ice and oil was insufficient for automatic segmentation. Segmentation was performed manually using the Wand Tool in ImageJ. Oil inclusions were selected by tracing objects. Therefore an initial pixel (iP) value was chosen for each oil bubble in the acquired 2-D slices. The Wand Tool checked the 4 neighbouring pixels of the iP. If the adjoining pixel was within the tolerance range of 3-5 of the iP value, it was detected as oil and its neighbouring pixels were checked in the same manner. If one pixel did not fulfil the criterion of falling into the range of the iP value, it was not accounted longer for oil and a border was set. Manual selection of oil was repeated on every 5^{th} to 20^{th} slice of an image stack. The selected areas were interpolated between the 2-D slices with the Region of Interest (ROI) manager and edited with the Segmentation Editor (Schindelin et al., 2012) giving a 3-D view of the oil inclusion. Segmentation results in 3-d images, where any voxel is either air, ice, oil or brine. The respective volume fraction were computed by GeoDict(2017).

The brine volume fraction Vb_{CT} was used to estimate the bulk sea ice salinity S_{CT} from

$$S_{CT} = \frac{S_b * \rho_b * Vb_{CT}}{\rho_i} \qquad (1)$$

where S_b is the brine salinity at imaging temperature, ρb is the brine density at imaging temperature and ρi is the bulk sea ice density. Sb 177.96 ppt was interpolated from the table given by Cox and Weeks (1983), ρb was taken as $1000+0.8Sb$ and bulk sea ice density ρi $[kgm^{-3}]$ was computed from CT- data, knowing the analyzed volume as well as the ice, air, oil and brine fractions. For pure ice the density of 920 kgm^{-3} was assumed.

Oil density was estimated as 877 kgm^{-3} from measured Crude oil Troll B density of 0.879 Mgm^{-3} at a temperature of 20 °C, assuming a linear increase of oil density with 0.01 Mgm^{-3}/15 °C. The oil volume fraction Vo_{CT} was converted to oil mass fractions by multiplication with $\rho oil/\rho i$.

Salinity and oil content of melted samples

Bulk salinity S of melted samples is based on electric conductivity measurements. Conversion from conductivity to ppt were conducted with the Gibbs Sea Water (GSW) Oceanographic Toolbox of TEOS- 10 (Dougall et al. 2011).

The mass fraction $Mo_{Fluroescent}$ oil in the melted samples was extracted with heptane by adding an equal volume of heptane to oil-containing samples. The concentration of oil in the heptane was subsequently analysed using a UV-fluorescence meter TD500™ (Turner Designs Hydrocarbon Instruments, Inc). Under UV or near UV light, aromatic hydrocarbons in the oil are stimulated or excited to fluoresce. The intensity of fluorescent emission reflects the concentration of aromatic hydrocarbons in the oil. Since the UV-fluorescence meter was calibrated with the same crude oil, the intensity of fluorescent emission corresponds to the concentration of the oil (Brost et al., 2011).

RESULTS

In our laboratory experiment columnar sea ice grew over the course of 91.5 hours to a thickness of 11-13 cm at an air temperature of -15 °C. 63.75 hour after the experiment start, ice thickness reached 8 cm and oil was released. Four lenses of Troll B crude oil were injected under the ice, each with a volume of 20-25 ml and a thickness of approximately 4 mm. Injected oil migrated along the ice-water interface before it collected at the highest points of small under-ice undulations.[1] Within 4 hours, a thin rim of horizontal platelets formed around the oil lenses. After 5.5 hours, a thin layer of ice platelets had formed beneath all four oil lenses. Ice cores were taken was taken when the ice layer underneath the oil lenses was 2-3 cm and an overall thickness of 11- 13 cm. Table 1 summarizes the analysis of cores taken as described in the method section and presented in the following figures.

[1] Phenomena of oil collecting in concave under- ice cavities and encapsulation process are for e.g. described by Glaeser & Vance (1971), NORCOR (1975), Goodman and Fingas (1983) Buist et al. (1983) and Wilkinson et al. (2007).

Air fraction

CT- based results for total and closed air volume are given for both acquisitions at SLF and at NTNU and are compared with each other in Figure 1. Open porosity is defined by a continuous path from the pore to one of the surface edges in x-, y-, or z- direction, whereas closed pores are not connected to any surface.

Total and closed air volume fraction Va_{SLF} and Va_{NTNU} are plotted in % over the ice thickness [cm] for cores C,D,E and F each with a length of 13, 12,11 and 12 cm. Air porosity for sample C4 is not shown in Figure 1 as Va_{SLF} and Va_{NTNU} the sample broke during transport. Therefore different areas were analysed resulting in a significant variance for Va_{SLF} and $Va_{NTNU.}$ Results from Closed air porosities in NTNU-acquisition excluding samples with oil lenses tend to be with a mean of 0.60% and a standard deviation of 0.23% higher than results from SLF with a mean of 0.52% and a standard deviation of 0.16%.

Brine fraction and salinity

Comparison of estimated bulk salinity S_{SLF} and S_{NTNU} determined from Vb_{SLF} and Vb_{NTNU} with measured bulk salinity S are shown for each core over the ice thickness in Figure 2. Salinity profiles show a characteristic C-Shape profile (Eicken, 1992). All salinity derived from µ-CT measurements is compared with direct measurements in Figure 4(a). Salinity calculation for S_{SLF} differs from direct measurements with a root mean square deviation of 1.64 %. S_{NTNU} differs from measurements with a root mean square error of 2.10 % from measured salinity.

Oil fraction

Oil content for samples imaged at the SLF and NTNU are expressed in oil mass fraction [%] to be comparable with fluorescent measurements (Figure 3 & 4). Oil injection level is highlighted in the plots at an ice thickness of 8 cm. Measurements displayed with a black circle, correspond to highlighted results in Table 1. The highest oil volume was found in sections close to the injection levels, i.e. at and near the location of the oil lenses. Results of oil content Mo_{SLF} and Mo_{NTNU} are compared with fluorescent oil content measurements in Figure 4. Differences between Mo_{NTNU} and $Mo_{Fluorescenct}$ are given by a root mean square deviation of 0.76%. Mo_{SLF} deviates from fluorescent measurements $Mo_{Fluorescence}$ with a root mean square error of 1.27%. While µ -CT measurements seem to be biased slightly high or low, agreement with fluorescent measurements is very good. With the notable exception of C4 acquired with a resolution of 18 µm. Oil and ice absorption contrast was too low in the mentioned sample for visual detection.

Table 1: Summary of key parameters and experiment results.

Sample	Sample Depth from air-ice interface	Air Volume Fraction (SLF) Va_{SLF}		Air Volume Fraction (NTNU) Va_{NTNU}		Brine Volume Fraction (SLF) Vb_{SLF}		Brine Volume Fraction (NTNU) Vb_{NTNU}		Bulk Salinity S_{SLF} from Vb_{SLF}	Bulk Salinity S_{NTNU} from Vb_{NTNU}	Bulk Salinity S	Oil Mass Fraction (SLF) Mo_{SLF}	Oil Mass Fraction (NTNU) Mo_{NTNU}	Oil Mass Fraction (Fluorescent) $Mo_{Fluorescent}$
-	cm	%		%		%		%		ppt	ppt	ppt	%	%	%
-	-	total	closed	total	closed	total	closed	total	closed			-	-	-	-
C1	0-2.5	-	-	3.42	0.99	-	-	4.94	3.69	-	10.9	6.8	-	0.00	-
C2	2.5-3.5	-	-	0.57	0.51	-	-	3.34	2.34	-	7.4	5.1	-	0.00	-
C3	3.5-6	0.89	0.61	0.95	0.58	2.61	2.30	2.18	1.97	5.8	4.8	6.4	0.44	0.47	0.57
C4	6-8.5	26.45	0.19	0.65	0.12	2.54	1.99	4.09	2.27	5.6	9.0	5.3	0.98	0.00	1.19
D1	0-2.5	-	-	0.79	0.71	-	-	3.54	2.5	-	7.8	6.7	-	0.00	-
D2	2.5-5	0.63	0.48	0.60	0.50	3.66	2.77	3.04	2.44	8.6	6.7	6.4	0.008	0.01	0.02
D3	5-7.5	1.76	0.85	4.54	3.75	3.49	2.99	1.94	1.63	7.7	4.3	5.9	10.09	8.61	6.74
D4	7.5-11	-	-	0.48	0.44	-	-	4.72	4.22	-	10.4	9.1	-	0.00	0.56
E1	0-2.5	-	-	1.26	0.95	-	-	3.47	2.71	-	7.7	6.8	-	0.00	
E2	5-7.5	0.61	0.52	0.66	0.58	4.01	3.30	2.85	0.62	8.9	6.7	5.8	0.09	0.04	0.12
E3	7.5-10	0.97	0.67	1.04	0.55	3.10	2.75	1.61	1.53	6.9	3.6	5.3	1.39	0.72	0.73
E4	10-11.5	5.81	0.78	-	-	2.35	1.98	-	-	5.2	-	6.9	4.77	-	3.09
F1	0-2.5	-	-	6.38	0.78	-	-	2.79	2.07	-	6.2	7.1	-	0.00	-
F2	2.5-5	0.86	0.66	0.84	0.72	2.85	2.33	1.36	1.23	6.3	3.0	5.5	0.12	0.02	0.10
F3	5-8	4.47	1.05	3.60	3.52	2..40	2.18	1.85	1.54	5.3	4.2	4.5	6.88	5.07	-
F4	8-10	-	-	0.59	0.36	-	-	4.69	3.26	-	10.4	7.1	0.00	0.00	-

Temperature [°C]	Brine Density ρb [Mgm^{-3}]	Brine Salinity Sb [ppt]	Oil Density [Mgm^{-3}]
-15	1.14236	177.95	0.877

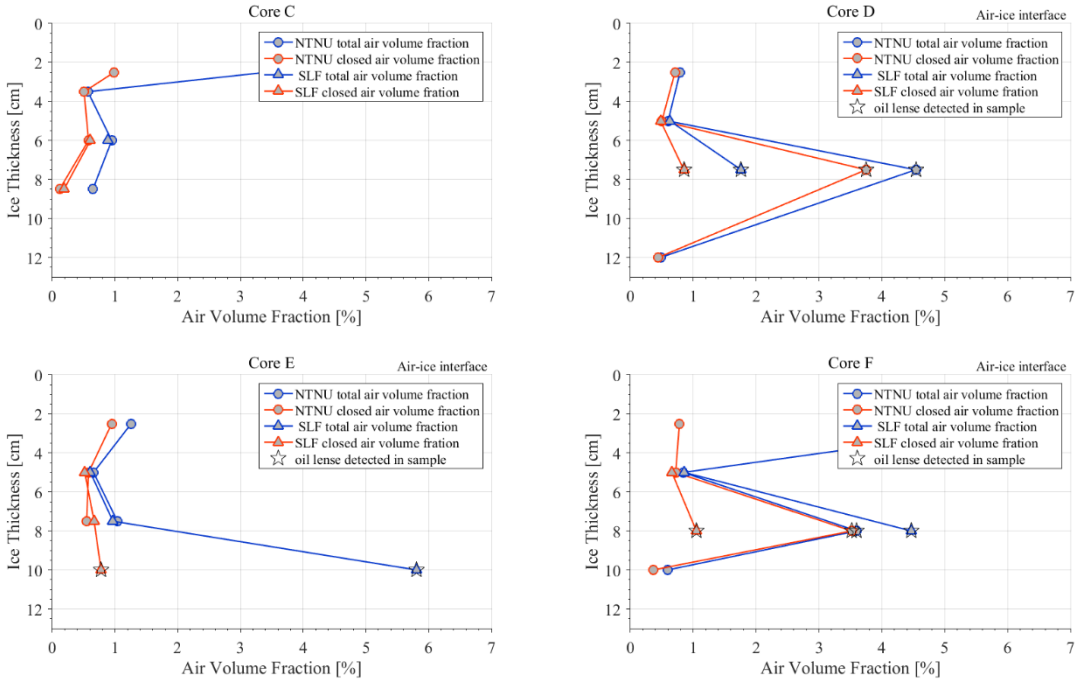

Figure 1: Closed and total air volume fraction from µ-CT- scans at SLF and NTNU in comparison.

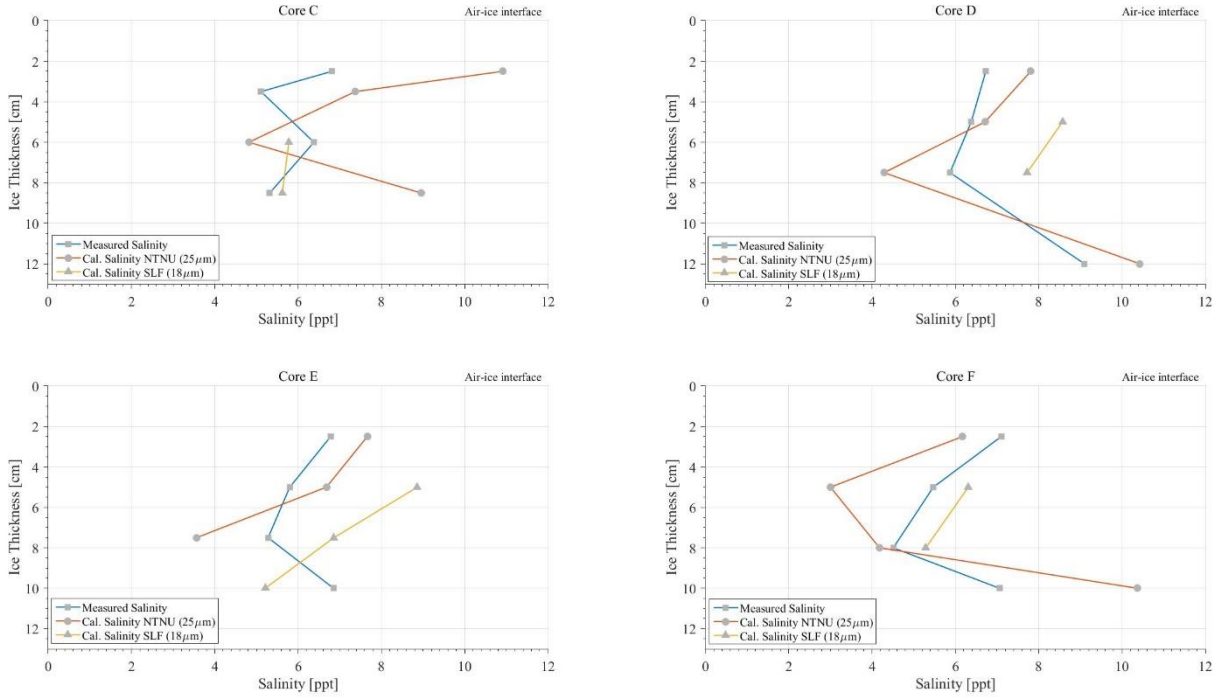

Figure 2: Measured bulk ice salinity in comparison with approximated bulk salinity based on segmented brine volume fractions of SLF-scans and NTNU-scans.

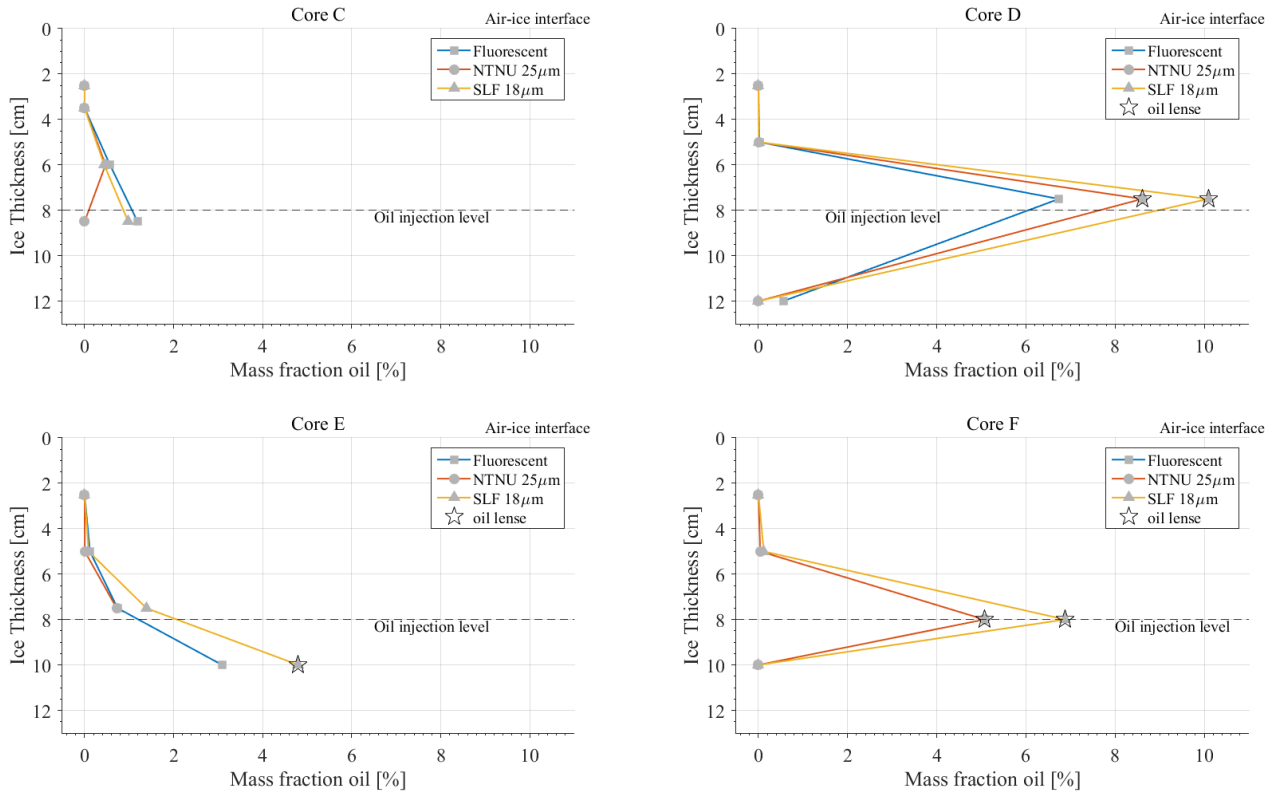

Figure 3: Oil content expressed in mass fraction in comparison between fluorescent measurement, µ-CT images from SLF and NTNU. Results highlighted with a black circle are averaged over the whole volume.

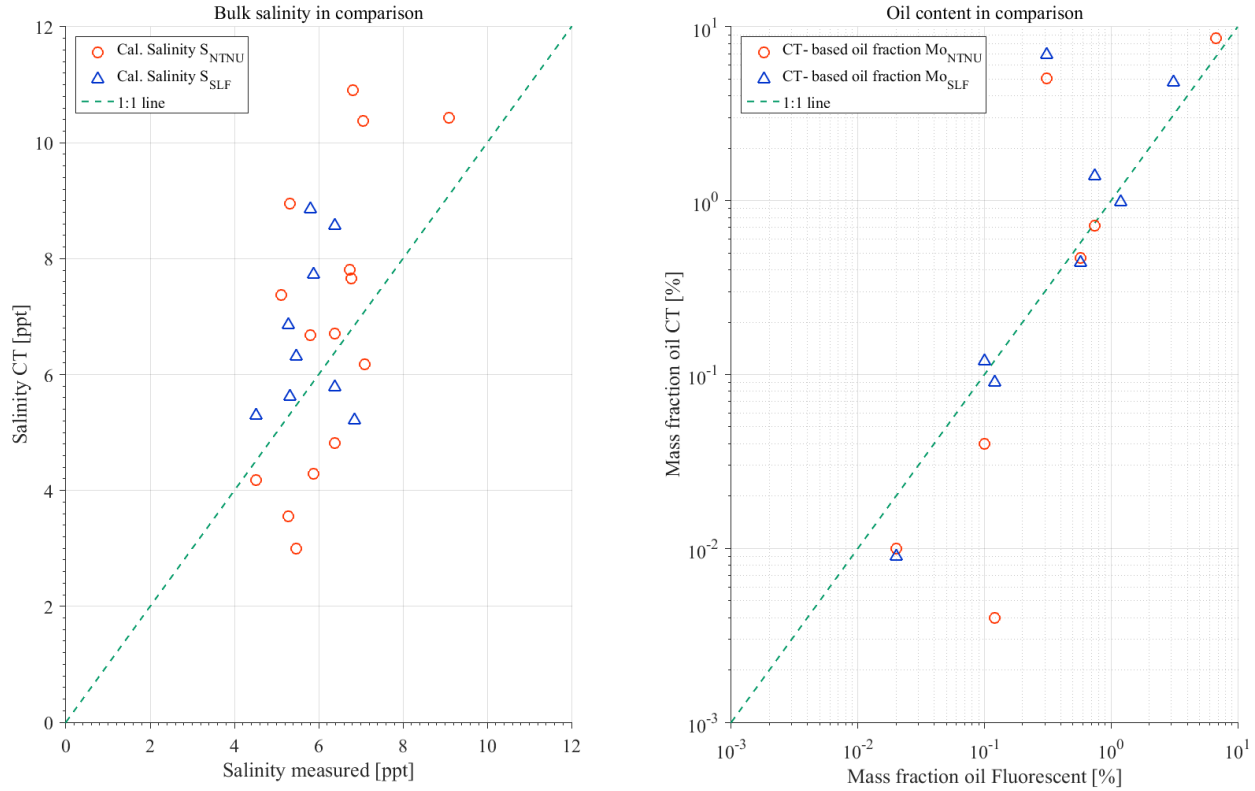

Figure 4: Bulk salinity of three different sources CT-scans (NTNU), CT-scans (SLF) and measured in comparison; Oil content from CT-scans (NTNU), CT-scans (SLF) and fluorescent in comparison.

DISCUSSION

Air fraction

Air segmentation with Otsu algorithm gives reasonable and consistent results for SLF and NTNU scans in comparison (Fig. 1). Total porosity is influenced by the open porosity, which might result from brine drainage. Values for closed porosity are there for more reliable. Spikes in air volume fraction are observed for samples containing oil concentrated in lenses (Figure 1), with one exception for sample F1. Sample F1 shows higher air content in the top most part. Observed air volume are open pores, indicating that potentially brine was leaking during sampling, storage and transportation.

We noticed larger air volumes above all oil lenses. Samples F3 and D3 where sectioned in a way, that preserved the closed air volume forming channels above the oil lens (Figure 6). Air volumes of 73.6 and 226.3 mm^3, respectively were found. Additionally smaller air bubbles were detected within the lenses of oil with a volume of 1 to 3 mm^3. However, we cannot be sure whether these are real due to air content of the oil or resulting from thermal cycling.

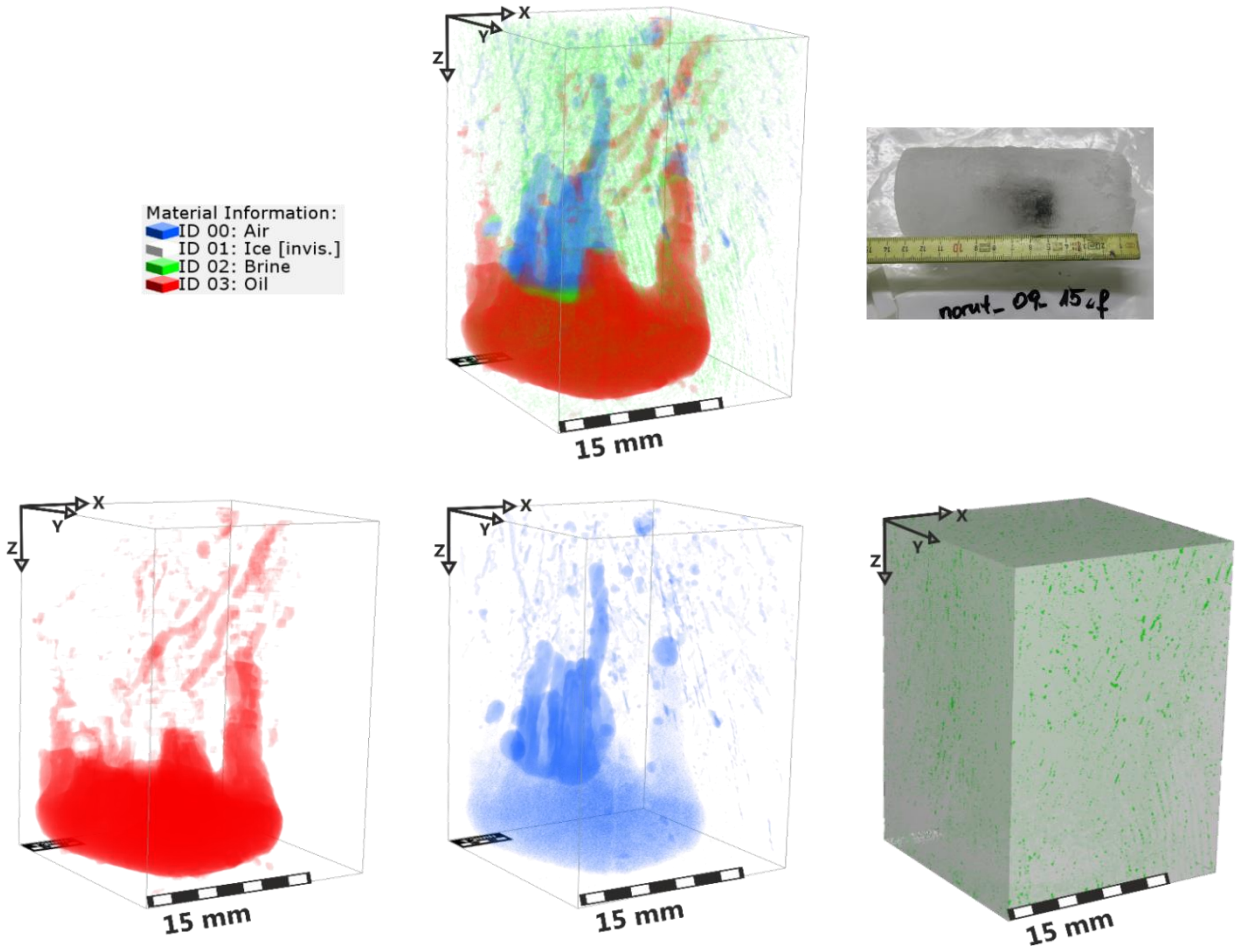

Figure 5: 3-D image of segmented oil (red) air (blue) and brine (green) for sample F3 resulting from µ-CT at SLF. Ice is invisible, except of the last image where ice is shown in white.

Too high closed air porosities in sample F3 and D3 from images at NTNU are observed in comparison to SLF data. Short thermal cycles above –15 °C might have occurred during scanning at SLF. As the temperature in the CT was controlled over the room temperature in the cold lab. Exposure to temperatures above the crude oil pour point (-15 °C) might lead to oil migration and drainage within the sample. Consequently the initial oil filled space is replaced by air. By cooling the sample afterwards down to the transport temperature, refreezing processes start and leave a closed pore.

While the source of these volumes could not been established unambiguously candidates include:

a. Unintended air release during first oil injection.
b. Air collected by the oil droplets migrating beneath the ice prior to freeze-in leading to an estimated air volume of 300 mm^3, for a prior freeze migration length of 10 mm by an oil lens diameter of 20 mm;
c. fluid loss during repeated warming and cooling cycles.

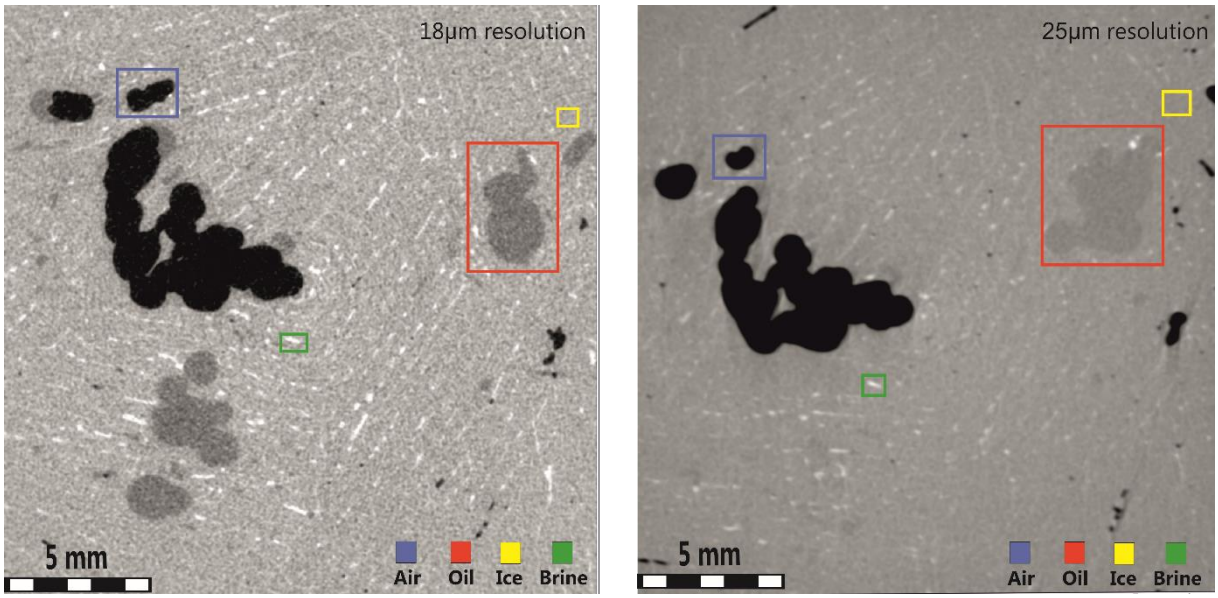

Figure 6: 2-D sections 18 µm respectively 25 µm resolution. Showing typical grey values for air, oil, ice and brine.

Brine fraction and salinity

CT- based salinity evaluation results in comparison to measured salinity in an error of approximately 2% (Fig. 4). Where S_{SLF} shows a slightly higher salinity than S_{NTNU}. Error can possibly result from different:

(a) chosen energy setting for SLF and NTNU acquisition. Higher energy resolve the ice to brine contrast better, resulting in higher evaluated salinity. Furthermore, plastic sample holder (SLF) with a lower X-ray absorption in comparison to aluminum holder (NTNU) were chosen, having a possible effect on the results. Systematically evaluation on a bigger data set is needed to determine influences.
(b) pixel size of 25 µm and 18 µm results in resolving objects ≥ 50 µm and 36 µm

respectively, i.e. 2x pixel size. This assumption would lead to an higher estimated salinity for smaller pixel sizes. Relevance of resolution for brine volume segmentation is not certain.

(c) imaging temperature was chosen to be -15°C for both acquisitions, the actual temperature in the CT at the SLF, was controlled over the room temperature and might therfore be slightly different.

Oil fraction

Manual oil segmentation is time consuming and subjective. Figure 5 shows the air, brine, and oil distribution in sample F3 acquired at the SLF. In general, most oil was found a few mm underneath and above the respective oil injection level. Above the oil lenses, oil was found in channels with a similar orientation to the brine layer direction and as individual, tiny oil pockets. Oil was detected in inclusions as small as 0-36 μm in images acquired at SLF. Whereas observation of acquisition NTNU show that the smallest oil inclusions was found in pockets with a diameter in between 0- 50 μm, which is actually 2x the pixel size. Largest inclusion was found in a pore with 19 mm in diameter. Oil migration was observed up 2.5 to 5 cm above the respective lenses. Where oil was detected in the lower third up to 2/3 of the sample, approximately to a level 4 cm from the air- ice interface. I.e., within 46 hours oil migrated approximately 4 cm upwards from the oil injection level.

Oil content in CT- data in comparison with fluorescence measurements tend to be higher for samples with oil lenses and underestimated for samples with smaller oil inclusions.Inclusions were classified as oil only if they appeared over more than one slice. More objective results could be expected from automated segmentation. However, this was not possible in the current experiments since the oil and ice absorption contrast was too low. Enhancement of the oil-ice contrast could be achieved by doping the oil, e.g. with iodoheptane (Brown et al., 2014).

The oil content compared in Figure 3 shows that trends were consistent. However, Vo_{SLF} tends to be higher than Vo_{NTNU}. Observed trend can be explained by several factors:

a. due to subjective manual segmentation and the tendency to discard doubtful oil signals, just appearing in a single slice
b. Lower resolution data do show a coarser vertical grid, smaller inclusions were therefore easier excluded and accounted for ice;
c. choice of energy during CT-acquisition show a significant effect on the oil detectability (Fig.6), lower energies used for acquisition at 18 μm result in a higher absorption contrast between oil and ice, and are easier to detect.
d. oil loss and drainage during transport and acquisition at SLF.

CONCLUSIONS

μ-CT is a powerful instrument to obtain non-destructive 3-dimensional insights into the interior of sea ice. The employed laboratory CTs provide satisfying results on low absorption contrast materials such as sea ice and oil (Figure 6) and reveal their spatial distribution (Figure 4).

Automated segmentation for air with the Otsu gave reasonable results for oil free samples with small bias in vertical profiles. Comparison of salinity evaluated from CT-data with measured salinity show a slight overestimation of brine volume fractions.

Spatial distribution of oil can be studied with significant investment of time into manual segmentation. Oil was found in inclusions with a diameter as small as 0- 36 μm, i.e actually 2

times pixel size. Comparisson of oil content from μ-CT with fluorescent measurements show consistent trends.Future motivation is given by the improvements in segmentation to open the possibility for quantitative oil and ice studies.

ACKNOWLEDGEMENTS

We gratefully acknowledge Matthias Jaggi for assistance and expertise at WSL Swiss Federal Institute for Snow and Avalanche Research SLF, as well as Ole Tore Buset and Leander Michels for guidance and help during μ-CT measurements at the Norwegian University of Science and Technology (NTNU). Special thanks to Math2Market, GeoDict for providing us with the imaging analysis software. Much appreciation to Statoil for providing Troll B crude oil. This work was supported by the Research Council of Norway PETROMAKS2 program, project number 243812 (MOSIDEO).

REFERENCES

Buist, I. A., Potter, S., & Dickins, D. (1983). Fate and Behaviour of Water-in-Oil Emulsion in Ice. *Proceedings of the 6th Annual AMOP Technical Seminar, 263-279.*

Brost, D. F., Foster, A. E., Holmes, M., Designs, T., & Instruments, H. (2011). No-Solvent Oil-in-Water Analysis – A Robust Alternative to Conventional Solvent Extraction Methods. *Offshore Technology Conference*, (January 2011), 1–18. http://doi.org/10.4043/21695-MS

Brown, K., Schlüter, S., Sheppard, A., & Wildenschild, D. (2014). On the challenges of measuring interfacial characteristics of three-phase fluid flow with x-ray microtomography. *Journal of Microscopy*, *253*(3), 171–182.

Buist, I. A., & Pistruzak, W. M. (1981). Dome Petroleum's Oil and Gas Undersea Ice Study. In *Proceedings of the Arctic Marine OIl Spill Programm Technichal Seminar, Edonton, Alberta*.

Cox, G. F. N., & Weeks, W. F. (1983). Equations for determining the gas and brine volumes in sea - ice samples. *Journal of Glciology*, *29*(102), 306–316.

Eicken, H. (1992). Salinity Profiles of Antarctic Sea Ice : Field Data and Model Results. *Journal of Geophysical Research,* 97(C10), 15545-15557

Glaeser, J. L., & Vance, G. P. (1971). *A Study of Behaviour of Oil Spills in the Arctic*.

Hullar, T., & Anastasio, C. (2016). Direct visualization of solute locations in laboratory ice samples. *The Cryosphere*, 10(5), 2057-2068

Karlsson, J. (2009). Oil Movment in Sea Ice, A laboratory study of fixation , release rates and small scale movement of oil in. *University of Copenhagen, Copenhagen,Denmark.*

Karlsson, J., Petrich, C., & Eicken, H. (2011). OIL ENTRAINMENT AND MIGRATION IN LABORATORY- GROWN SALTWATER ICE. In *Proceedings of the 21st International Conference on Port and Ocean Engineering under Arctic Conditions, Montreal ,Canada*.

Kawamura, T. (1988). Observations of the internal structure of sea ice by X ray computed tomography. *Journal of Geophysical Research*, *93*(C3), 2343.

Martin, S. (1979). A field study of brine drainage and oil entrainment in first-year sea ice. *Journal of Glaciology*, *22*(88), 473–502.

Maus, S. (2009). Synchrotron-based X-ray micro-tomography: Insights into Sea Ice

Microstructure.*Report Series in Geophysics, Proceedings of The Sixth Workshop on Baltic Sea Ice Climate*.

Maus, S., Becker, J., Leisinger, S., Matzl, M., Schneebeli, M., & Wiegmann, A. (2015). Oil Saturation of the Sea Ice Pore Space. In *Proceedings of the 23rd International Conference on Port and Ocean Engineering under Arctic Conditions, Trondheim, Norway*.

Maus, S., Leisinger, S., Matzl, M., Schneebeli, M., & Wiegmann, A. (2013). Modelling oil entrapment in sea ice on the basis of 3d micro-tomographic images. In *Proceedings of the 22nd International Conference on Port and Ocean Engineering under Arctic Conditions, Espoo, Finnland*.

McDougall, T. J., & Barker, P. M. (2011). Getting started with TEOS-10 and the Gibbs Seawater (GSW) oceanographic toolbox. SCOR/IAPSO WG, 127, 1-28.

Nelson, W. G. (1981). Oil Migration and Modification Processes in Solid Sea Ice. *International Oil Spill Conference, American Petroleum Institute*, *1*.

NORCOR, (1975). The Interaction of Crude Oil With Arctic Sea Ice.*NORCOR Engineering and Research Limited Yellowknife, N.W.T.*, Beauforts Sea Technical Report 27

Otsu, N. (1979). A Threshold Selection Method from Gray-Level Histograms. *IEEE Transactions on Systems, Man, and Cybernetics*, *9*(1), 62–66.

Otsuka, N., Kondo, H., & Saeki, H. (2004). Experimental study on the characteristics of oil ice sandwich. In *Oceans '04 MTS/IEEE Techno-Ocean '04 (IEEE Cat. No.04CH37600)* (Vol. 3, pp. 1470–1475).

Petrich, C., Karlsson, J., & Eicken, H. (2013). Porosity of growing sea ice and potential for oil entrainment. *Cold Regions Science and Technology*, *87*, 27–32.

Schindelin, J., Arganda-Carreras, I., Frise, E., Kaynig, V., Longair, M., Pietzsch, T., … Cardona, A. (2012). Fiji: an open-source platform for biological-image analysis. *Nature Methods*, *9*(7), 676–682. http://doi.org/10.1038/nmeth.2019

Timco, G. W., & Weeks, W. F. (2010). A review of the engineering properties of sea ice. *Cold Regions Science and Technology*, *60*(2), 107–129.

Wilkinson, J. P., Wadhams, P., & Hughes, N. E. (2007). Modelling the spread of oil under fast sea ice using three-dimensional multibeam sonar data. *Geophysical Research Letters*, 34(22).

Zack, G. W., Rogers, W. E., & Latp, S. A. (1977). Automatic Measurement of Sister Chromatid Exchange Frequency. *The Journal of Histochemistry and Cytochemistry*, *25*(7), 741–753.